

RASR: Retrieval-Augmented Super Resolution for Practical Reference-based Image Restoration

Jiaqi Yan^{1,3*}, Shuning Xu^{2,3}, Xiangyu Chen^{3†}, Dell Zhang³, Jie Tang¹, Gangshan Wu¹, Jie Liu^{1†}

¹ State Key Laboratory for Novel Software Technology, Nanjing University,

² State Key Laboratory of Internet of Things for Smart City,

Department of Computer and Information Science, University of Macau,

³ Institute of Artificial Intelligence (TeleAI), China Telecom

jiaqi_yan@smail.nju.edu.cn, {rebeccaxu0418, chxy95}@gmail.com, dell.z@ieee.org, {tangjie, gswu, liujie}@nju.edu.cn

Abstract

Reference-based Super Resolution (RefSR) improves upon Single Image Super Resolution (SISR) by leveraging high-quality reference images to enhance texture fidelity and visual realism. However, a critical limitation of existing RefSR approaches is their reliance on manually curated target-reference image pairs, which severely constrains their practicality in real-world scenarios. To overcome this, we introduce Retrieval-Augmented Super Resolution (RASR), a new and practical RefSR paradigm that automatically retrieves semantically relevant high-resolution images from a reference database given only a low-quality input. This enables scalable and flexible RefSR in realistic use cases, such as enhancing mobile photos taken in environments like zoos or museums, where category-specific reference data (e.g., animals, artworks) can be readily collected or pre-curated. To facilitate research in this direction, we construct RASR-Flickr30, the first benchmark dataset designed for RASR. Unlike prior datasets with fixed target-reference pairs, RASR-Flickr30 provides per-category reference databases to support open-world retrieval. We further propose RASRNet, a strong baseline that combines a semantic reference retriever with a diffusion-based RefSR generator. It retrieves relevant references based on semantic similarity and employs a diffusion-based generator enhanced with semantic conditioning. Experiments on RASR-Flickr30 demonstrate that RASRNet consistently improves over SISR baselines, achieving +0.38 dB PSNR and -0.0131 LPIPS, while generating more realistic textures. These findings highlight retrieval augmentation as a promising direction to bridge the gap between academic RefSR research and real-world applicability.

Introduction

Single Image Super Resolution (SISR) aims to reconstruct a high-resolution (HR) image from a single low-resolution (LR) input, striving to recover perceptually plausible and visually realistic textures. Recent advances, from CNN-based models (Zhang et al. 2021; Wang et al. 2021) to transformer architectures (Liang et al. 2021; Chen et al. 2023), and diffusion-based generative models (Wang et al. 2024a; Wu et al. 2024b; Yu et al. 2024), have significantly improved the

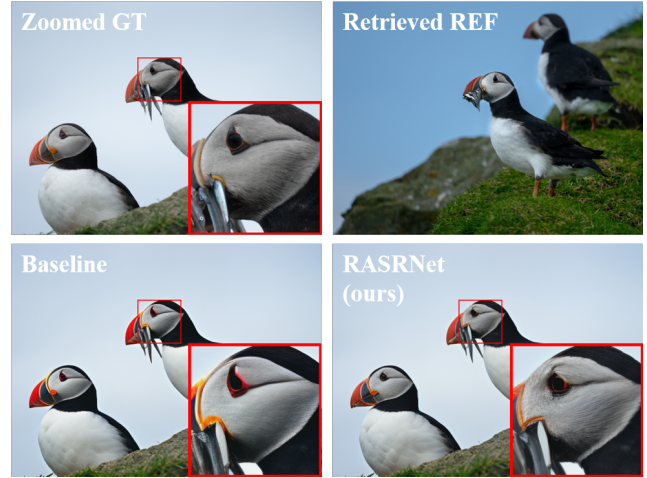


Figure 1: Visual comparison between RASRNet and the SISR baseline. Our method generates more realistic textural details (e.g., the Atlantic puffin’s eye) using a reference image retrieved from the RASR-Flickr30 database.

perceptual quality and fidelity of SISR results. Despite these improvements, SISR remains inherently ill-posed and often struggles to hallucinate fine-grained textures, particularly in regions with complex or ambiguous content.

To address the limitations of SISR, Reference-based Super Resolution (RefSR) has emerged as a compelling alternative. By leveraging auxiliary high-quality reference images that share semantic or structural similarity with the LR input, RefSR methods (Jiang et al. 2021; Cao et al. 2022; Zhang et al. 2023) can transfer realistic textures and recover intricate visual details that SISR models alone typically fail to reconstruct. Despite their potential, existing RefSR approaches typically rely on manually curated target-reference image pairs, an assumption that severely limits their scalability and real-world applicability. In practice, users rarely have access to such perfectly paired references at inference time, and how to efficiently acquire suitable reference images remains an underexplored challenge.

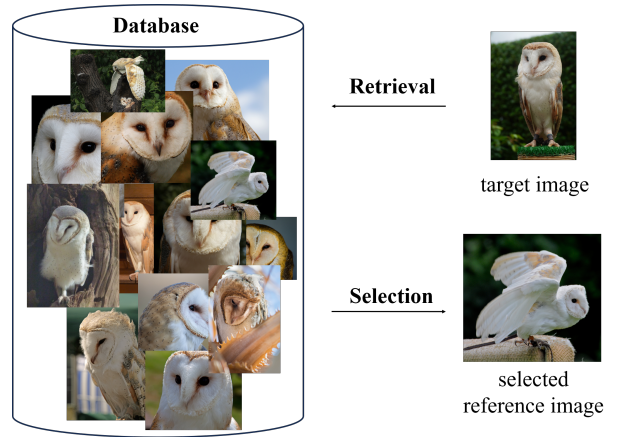
In this work, we propose Retrieval-Augmented Super Resolution (RASR), a new and practical RefSR paradigm

*This work was done during the author’s internship at TeleAI.

†Corresponding Author.



(a) RASR-Flickr30 Dataset preview



(b) Retrieval process

Figure 2: (a) Example images from the proposed RASR-Flickr30 dataset. (b) Illustration of the retrieval process, where a target image queries the database to identify the most semantically relevant reference for RASR.

that removes the need for manual reference pairing. Given only an arbitrary LR input, RASR automatically retrieves semantically relevant HR images from a large-scale reference database, enabling flexible and scalable RefSR deployment. Importantly, we observe that in many real-world scenarios, high-quality reference databases are naturally available or can be pre-defined. For example, in specific visual environments such as zoos, museums, or exhibitions, it is often feasible to pre-collect reference images of common subjects—such as animals, artifacts, or artworks—which can then be reused across different user inputs. In such closed or category-specific domains, RASR becomes particularly advantageous, offering a practical solution for enhancing photos captured in these contexts.

To support research in this new direction, we introduce RASR-Flickr30, the first benchmark dataset explicitly designed for RASR. Unlike prior datasets with fixed target-reference pairs, RASR-Flickr30 provides per-category reference galleries, enabling open-world and dynamic retrieval (see Fig. 2). This design better reflects practical use cases, where reference collections are organized by semantic class and retrieval must adapt to the content of the input image. Furthermore, we present RASRNet, a strong retrieval-to-generation baseline for RASR. It integrates: (1) A semantic retriever that efficiently selects relevant high-resolution references based on class-level similarity; and (2) A diffusion-based RefSR generator, built upon pretrained SISR-Diffusion backbones and augmented with semantic conditioning via ControlNet (Zhang, Rao, and Agrawala 2023). Unlike patch-based methods, our model leverages global semantic features from references, yielding robust and perceptually faithful reconstructions under diverse degradations. Our method is extensively validated through experiments and consistently produces more realistic and detailed textures (e.g., Fig. 1).

Our contributions are as follows:

- We propose Retrieval-Augmented Super Resolution, a new paradigm that expands RefSR applicability by en-

abling flexible reference retrieval.

- We present RASR-Flickr30, the first retrieval-augmented SR dataset, built with per-category reference databases that support dynamic and context-aware retrieval.
- We introduce RASRNet, a new method that outperforms SISR baselines and showcases the potential of reference retrieval in real-world super-resolution tasks.

Related Work

Diffusion-based Real Image Super Resolution

Diffusion models have recently achieved remarkable success in high-quality image generation, starting from unconditional generation to powerful text-to-image (T2I) models. Motivated by their strong generative capacity, researchers have explored applying T2I models to address super resolution problem. StableSR (Wang et al. 2024a) is an early approach that guides T2I model to generate promising outputs by introducing a time-aware encoder and a controllable feature wrapping module. DiffBIR (Lin et al. 2024) proposes first removing degradation and then using T2I model for information regeneration to tackle blind image restoration tasks. PASD (Yang et al. 2024) and SeeSR (Wu et al. 2024b) further utilize the semantic information to guide the diffusion process extracted from input by another image-to-text module. However, traditional diffusion models require many sampling steps and are computationally expensive. To address this, recent approaches such as SinSR (Wang et al. 2024b) and OSEDiff (Wu et al. 2024a) propose efficient sampling strategies or single-step generation frameworks, greatly improving inference speed while maintaining output quality. Beyond efficiency-focused methods, recent work such as RefFIR proposes a training-free framework that utilizes external references to reduce hallucination and expand the knowledge boundaries of large resolution models.

Reference-based Image Super Resolution

RefSR task aims to enhance image reconstruction by leveraging semantically similar high-quality reference images, offering significant advantages over SISR. Early works primarily focus on improving the effectiveness of correspondence matching between the target and reference images. One line of research (Zheng et al. 2018; Shim, Park, and Kweon 2020) leverages spatial alignment techniques, such as flow estimation or deformable convolutions (DCN) (Dai et al. 2017), to establish dense correspondences. Another line (Zhang et al. 2019a; Yang et al. 2020) employs patch-matching method (Barnes et al. 2009), capturing long-range correspondences. Recently, C^2 -Matching (Jiang et al. 2021) introduces teacher-student correlation distillation and combines patch-matching with DCN for alignment. DATSR (Cao et al. 2022) incorporates the Swin Transformer architecture (Liu et al. 2021) into RefSR, achieving improved performance. MRefSR (Zhang et al. 2023) introduces a simple yet effective baseline to support multiple reference inputs. Although superior to SISR (Wang et al. 2021; Liang et al. 2021), these methods rely on pre-paired references and patch-matching, which are impractical and unreliable for real-world degraded images (Wang et al. 2024a). Therefore, developing methods that can efficiently retrieve appropriate references for a target image and effectively aggregate reference information into the output without relying on precise patch matching remains an important and underexplored problem. This work aims to address these challenges.

Reference-based Super Resolution Datasets

Existing datasets commonly used in RefSR researches include Sun80 (Sun and Hays 2012), Urban100 (Huang, Singh, and Ahuja 2015), Manga109 (Matsui et al. 2017), WR-SR (Jiang et al. 2021), CUFED5 (Zhang et al. 2019b) and LMR (Zhang et al. 2023). Sun80 provides 20 web-searched references per image, but with low relevance. Urban100 and Manga109 lack explicit references and rely on intra-image or random substitution. WR-SR contains 80 image-reference pairs with diverse content but limited scale. CUFED5 and LMR are the only existing RefSR datasets that provide training sets. However, CUFED5 suffers from a low resolution of only 160×160 and provides only a single reference image per input. LMR improves this by offering 300×300 training images with five reference images per group. Nevertheless, both datasets share common limitations: the resolution of training images remains too low for real-world applications and diffusion model training, and the reference images are pre-designed for each input, which is impractical in real scenarios where reference retrieval should be automatic. To address these limitations, we introduce RASR dataset RASR-Flickr30, which provides high-quality reference database images and supports open-set reference retrieval, making it more suitable for realistic RefSR tasks.

Methodology

Task Formulation: RASR

As detailed in the Introduction, traditional RefSR methods rely on manually curated target-reference pairs, limit-

ing their scalability and flexibility. To overcome these limitations, we propose Retrieval-Augmented Super Resolution (RASR), a new RefSR paradigm that automatically retrieves semantically relevant references from a reference database to guide the super resolution process for LR input I_{LR} . Formally, the RASR task is defined as:

$$\text{RASR}(I_{LR}) = \mathcal{G}(I_{LR}, I_{REF}) = \mathcal{G}(I_{LR}, \mathcal{R}(\mathcal{DB}, I_{LR})), \quad (1)$$

where \mathcal{DB} denotes a pre-curated database containing high-quality reference images, \mathcal{R} is a retriever that selects the most semantically relevant reference image I_{REF} from \mathcal{DB} based on I_{LR} , \mathcal{G} is a generation function that reconstructs HR output conditioned on both I_{LR} and I_{REF} .

RASR Network

RIRR: Real-world Image Reference Retriever

Reference retrieval remains an open problem with various approaches. Texture-based retrieval matches low-level patterns but is sensitive to noise and blur in real-world LR images, causing unreliable results. In contrast, semantic-based retrieval uses high-level features from vision encoders, offering more robust and generalizable matching despite degradations. We argue that semantic similarity-based retrieval is optimal for real-world RefSR, as it remains robust under severe degradations and allows flexible cross-instance references, thereby broadening RefSR applicability. As shown in Fig.3 (a), RIRR retrieves the most semantically relevant reference image for a given LR input. We first use a vision encoder (e.g., DINOv2 (Oquab et al. 2023)) to extract embeddings for all images in the reference database and store them as a searchable index. At inference time, we encode the LR input using the same vision encoder to obtain its embedding. Then, we perform nearest neighbor retrieval based on cosine similarity between the LR embedding and the reference embeddings. The retriever returns the reference image corresponding to the most similar embedding.

RefDSR: Reference Diffusion Super Resolution

Given a LR input image I_{LR} and a reference image I_{REF} retrieved from the reference database \mathcal{DB} , we propose a plug-and-play generator network \mathcal{G}_θ to produce a HR output image \hat{I}_{HR} . This network is designed to validate the effectiveness of the reference-based super-resolution paradigm within our retrieval-augmented generation framework.

Framework. We denote the VAE encoder, VAE decoder, and the latent diffusion network of a pretrained Diffusion model for SISR task as \mathcal{E} , \mathcal{D} , and \mathcal{F} , respectively. To preserve the original generative capability of the backbone, we freeze all parameters of the pretrained modules and introduce a trainable ControlNet (Zhang, Rao, and Agrawala 2023) branch, denoted as \mathcal{F}_θ^{REF} , as shown in Fig. 3 (b). In detail, we introduce lightweight, trainable components – LoRA (Hu et al. 2022) modules and train zero-convolution layers in the DownBlocks of \mathcal{F}_θ^{REF} . To encode I_{REF} into the latent space, we utilize a frozen VAE encoder \mathcal{E}^{REF} from a pretrained diffusion model. The encoded latent representation z_{REF} of the reference image is then fed into the ControlNet branch \mathcal{F}_θ^{REF} as the conditioning input. To obtain an un-

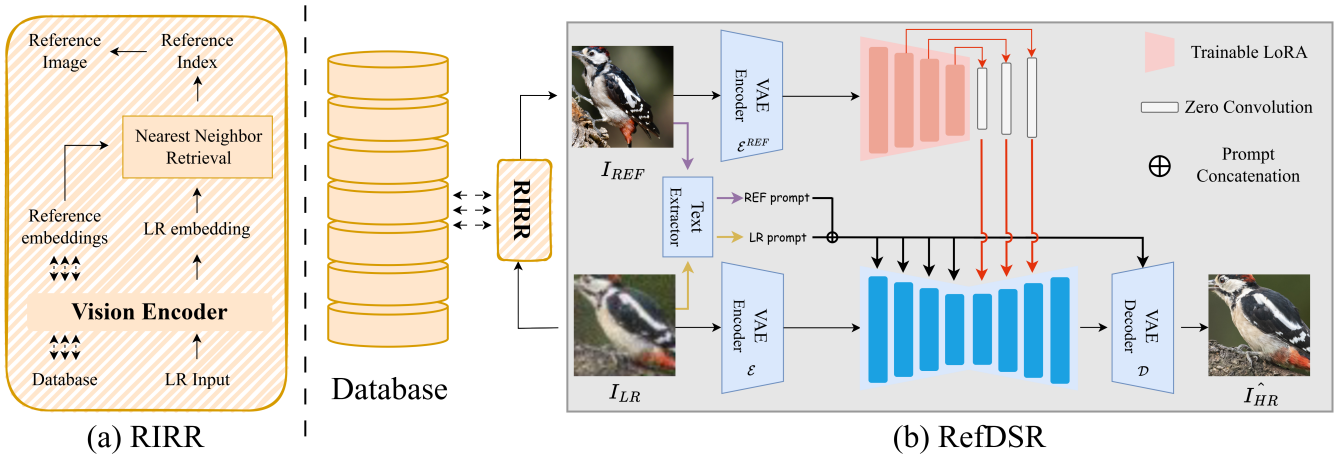


Figure 3: Overall architecture of RASRNet. It consists of two modules: Real-world Image Reference Retriever (RIRR) and Reference Diffusion Super Resolution (RefDSR). (a) RIRR comprises a vision retriever that identifies the most semantically similar reference image I_{REF} given a LR input I_{LR} . (b) RefDSR takes I_{LR} and I_{REF} as input. Text prompts extracted separately from I_{LR} and I_{REF} are concatenated as the text input for the UNet. I_{REF} is encoded by a frozen VAE Encoder \mathcal{E}^{REF} and processed by a LoRA-finetuned ControlNet to extract reference features. In the main pipeline, I_{LR} passes through the frozen encoder \mathcal{E} , UNet, and decoder \mathcal{D} without modification. Reference features are injected into the UNet decoder as additional conditions, replacing text cross-attention in the first three blocks.

conditioned latent representation of the reference image, we exclude text conditioning during its encoding.

The reference image provides semantic rather than structural similarity to the input, and injecting its features into shallow layers can mislead low-level reconstruction. In the vanilla ControlNet architecture, conditional features are injected into all decoder blocks, with text embeddings guiding the entire UNet via cross-attention. In contrast, our RefDSR model injects reference conditioning only into the first three decoder blocks (see Eq. 2), while text-based cross-attention is applied exclusively in the final decoder block. Here, f_{UNet}^i and $f_{ControlNet}^i$ denote the UNet and ControlNet features at block i , respectively. The updated UNet feature is:

$$\hat{f}_{UNet}^i = f_{UNet}^i + f_{ControlNet}^i, \quad i \in \{0, 1, 2\}. \quad (2)$$

Importantly, no text-based modulation is applied in these first three layers; only the ControlNet features are fused. This design ensures that the early decoding stages focus on reconstructing structural details under semantic guidance from the reference image, while global fidelity and style are refined by text conditioning at the final stage.

The reference diffusion process can be written as:

$$\begin{aligned} \hat{I}_{HR} &= \mathcal{G}_\theta(I_{LR}, I_{REF}, c_{text}) \\ &\triangleq \mathcal{D}(\mathcal{F}(\mathcal{E}(I_{LR}); \mathcal{F}_\theta^c(\mathcal{E}^c(I_{REF})); c_{text})), \end{aligned} \quad (3)$$

where c_{text} denotes the conditional text in the pretrained SISR Diffusion model.

Training Objectives. During training, we use an MSE loss, a perceptual LPIPS loss and a GAN loss, where the discriminator adopts a fixed DINO (Caron et al. 2021) backbone, following (Kumari et al. 2022). To generate sharper and more realistic details, we additionally adopt a Gram loss \mathcal{L}_{Gram} ,

defined as the L2 norm of the difference between the Gram matrices of VGG-16 features:

$$\mathcal{L}_{Gram} = \sum_{l \in \mathcal{L}} \lambda_l \frac{1}{C_l H_l W_l} \left\| G_l(I_{HR}) - G_l(I_{GT}) \right\|_2^2, \quad (4)$$

where $G_l(\cdot)$ denotes the Gram matrix computed from the feature maps at layer l , λ_l is the layer weight, and I_{GT} denotes the ground truth (GT) image.

The overall training loss is formulated as a weighted sum of the aforementioned terms:

$$\mathcal{L} = \mathcal{L}_{MSE} + \lambda_{LPIPS} \cdot \mathcal{L}_{LPIPS} + \lambda_{Gram} \cdot \mathcal{L}_{Gram} + \lambda_{GAN} \cdot \mathcal{L}_{GAN}, \quad (5)$$

where λ_{LPIPS} , λ_{Gram} , λ_{GAN} are the loss weights for each term.

Inference Process

During training, we use text prompts extracted from GT images. Although employing a fine-tuned text extractor during inference enhances performance, it remains unreliable in certain cases (Wu et al. 2024b). To address this, we propose using a combination of prompts extracted from the LR input and its retrieved reference during inference.

Besides, if the same fusion strategy as used during training is applied in the inference stage, although it achieves high fidelity, the perceptual quality tends to degrade. To obtain balanced results, we introduce a scalar weight of 0.5 within the fusion layers to adaptively balance the original and reference-modulated features. The fused output during inference is computed as:

$$\hat{f}_{UNet}^i = f_{UNet}^i + 0.5 \times f_{ControlNet}^i, \quad i \in \{0, 1, 2\}. \quad (6)$$

Method		PSNR \uparrow	SSIM \uparrow	LPIPS \downarrow	DISTS \downarrow	FID \downarrow	NIQE \downarrow	MUSIQ \uparrow	CLIQQA \uparrow
BSRGAN		24.72	0.5952	0.4399	0.2774	147.79	4.9689	54.36	0.5851
Real-ESRGAN	GAN-based	24.78	0.6078	0.4268	0.2694	124.53	4.9465	52.52	0.5373
HAT		25.07	0.6160	0.4007	0.2804	110.63	5.3254	48.20	0.4580
RAG- C^2 -Matching		24.40	0.5663	0.7004	0.3503	155.06	8.6838	17.97	0.1587
RAG-DATSR	Reference-based	24.41	0.5677	0.7052	0.3500	153.50	9.1758	17.99	0.1621
RAG-MRefSR		24.47	0.5753	0.7466	0.3395	153.25	9.9936	17.55	0.3004
StableSR		22.88	0.4867	0.3952	0.2147	87.74	4.3289	66.30	0.7083
DiffBIR		23.26	0.5144	0.4266	0.2236	109.57	5.0749	73.46	0.8366
PASD	Diffusion-based	23.97	0.5773	0.4724	0.2403	98.07	5.2452	61.61	0.6130
SeeSR		23.26	0.5515	0.3740	0.1919	72.97	4.4319	72.89	0.7987
OSDiff		23.29	0.5624	0.3404	0.1915	65.59	4.2009	71.35	0.7572
RASRNet (Ours)	RASR	23.67 <i>+0.38</i>	0.5687 <i>+0.0063</i>	0.3273 <i>+0.0131</i>	0.1743 <i>+0.0172</i>	56.83 <i>+8.76</i>	4.1139 <i>+0.0870</i>	72.33 <i>+0.98</i>	0.7706 <i>+0.0134</i>

Table 1: Quantitative comparison with state-of-the-art methods on RASR-Flickr30 test set.

RASR-Flickr30 Dataset

We propose RASR-Flickr30, a RASR dataset comprising high-quality target and reference database images constructed from publicly available images on Flickr.com¹. To reflect real-world scenarios where high-quality reference databases are readily available or easily constructed, we focus on animals. They provide natural visual diversity while maintaining consistent appearances within each species, making them well-suited for constructing reference databases with minimal intra-class variation. This setting aligns with the practical use cases of RASR in closed or category-specific domains.

Fig. 2 (a) previews sample images from RASR-Flickr30, illustrating the high-quality and category-consistent content within the dataset. Fig. 2 (b) illustrates the retrieval process enabled by the RASR-Flickr30 dataset, where a target image queries the database to identify the most semantically relevant reference.

Data Collection. We manually crawled and curated images from Flickr.com, with a focus on high-resolution, aesthetically pleasing animal photographs. We selected species with rich visual representation and sufficient image quantity. During the filtering process, we prioritized visual clarity, relevance of content, and photographic quality.

Diversity. RASR-Flickr30 covers 30 animal species, including both domestic and wild animals, with intra-class diversity in poses, backgrounds, lighting, and viewing angles. We ensure that each species has varied visual contexts to facilitate robust learning and generalization.

Partitions. For each species, 40 images are used for training and 5 for testing. The remaining images (approximately 100 per species) constitute the reference database used to support both retrieval and generation in the RASR framework.

¹<https://www.flickr.com/>

Experiments

Experiments Settings

Training and Testing Datasets. We train RefDSR on RASR-Flickr30 and the LSDIR (Li et al. 2023) dataset. For RASR-Flickr30, all training and reference database images are cropped into patches of size 768 \times 768. For each training sample, five reference images are pre-selected based on cosine similarity to the GT image. During training, one reference is randomly sampled from the five, and paired patches are randomly cropped to 512 \times 512. For the LSDIR dataset, two 512 \times 512 patches are randomly cropped from each image to form target-reference pairs, enhancing local diversity while maintaining global semantic consistency. For testing, we use the RASR-Flickr30 test set and the WR-SR (Jiang et al. 2021) dataset. To generate LR and HR training and testing pairs, we adopt the degradation pipeline from Real-ESRGAN (Wang et al. 2021).

Evaluation Metrics. For evaluation, we adopt both fidelity metrics (PSNR and SSIM) and perceptual metrics (LPIPS (Zhang et al. 2018), DISTS (Ding et al. 2020), and FID (Heusel et al. 2017)), along with several no-reference metrics (NIQE (Zhang, Zhang, and Bovik 2015), MUSIQ (Ke et al. 2021), and CLIPIQA (Wang, Chan, and Loy 2023)) to comprehensively assess the performance of different methods. Additionally, we conduct a user study presented in the supplementary material.

Implementation Details. To demonstrate the benefit of integrating reference information, we choose OSDiff (Wu et al. 2024a), a one-step-diffusion SISR model, as our baseline. We train RefDSR with the AdamW optimizer (Loshchilov and Hutter 2017) at a learning rate of 5e-5. The entire training process took approximately 33 hours on 4 NVIDIA A800 GPUs with a batch size of 24. For the ControlNet branch, we employ SD 2.1-base as the pretrained model and set the LoRA rank to 4. The weighting scalars λ_{LPIPS} , λ_{Gram} , and λ_{GAN} are set to 2, 1e-3 and 0.1, respectively.

Compared Methods. We compare our RASRNet with state-of-the-art GAN-based SISR methods, including BSRGAN (Zhang et al. 2021), Real-ESRGAN (Wang et al. 2021), and

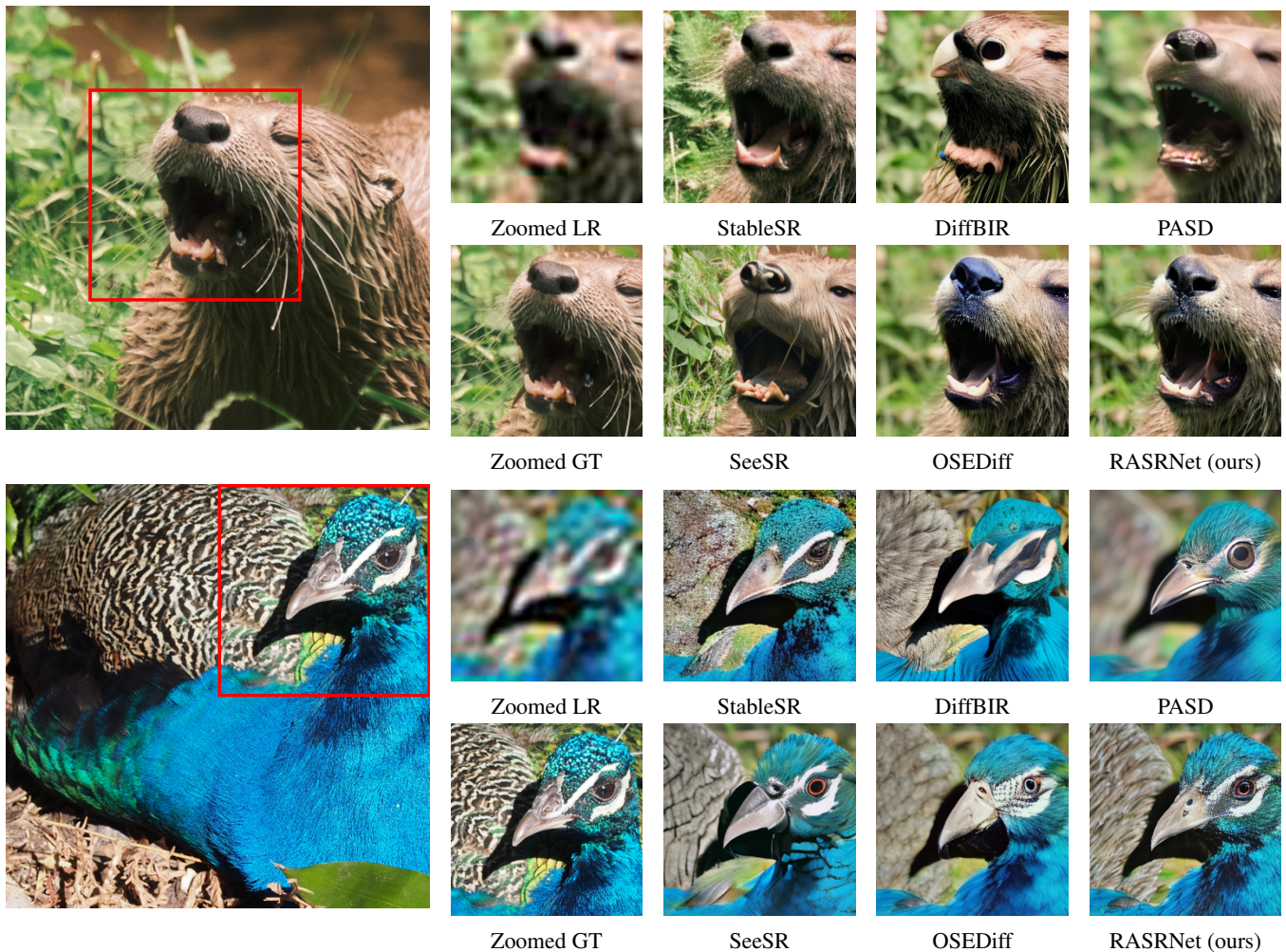


Figure 4: Qualitative comparisons of different diffusion-based SR methods.

HAT (Chen et al. 2023); RefSR methods, including C^2 -Matching (Jiang et al. 2021), DATSR (Cao et al. 2022), and MRefSR (Zhang et al. 2023); as well as diffusion-based methods, including StableSR (Wang et al. 2024a), DiffBIR (Lin et al. 2024), PASD (Yang et al. 2024), SeeSR (Wu et al. 2024b), and OSEDiff (Wu et al. 2024a).

Comparison with State-of-the-Arts

Quantitative Comparison. For the retrieval-based setting, we present quantitative comparisons on the synthetic RASR-Flickr30 test set in Tab. 1. For RefSR methods, we use the reference images retrieved by our RIRR module. We have the following observations: (1) Compared to the baseline OSEDiff, our RASRNet achieves consistent improvements across both full-reference and no-reference metrics. Specifically, it brings a PSNR improvement of +0.38 dB and an SSIM improvement of +0.0063. For perceptual metrics, it achieves reductions of -0.0131 in LPIPS, -0.0172 in DISTS, and -8.76 in FID, indicating enhanced visual fidelity and texture realism. In terms of no-reference metrics, RASRNet further improves NIQE by -0.0870 and achieves gains of +0.98

in MUSIQ and +0.0134 in CLIPQA. (2) Among all evaluated methods, RASRNet attains the best results on LPIPS (0.3273), DISTS (0.1743), FID (56.83), and NIQE (4.1139), demonstrating its superiority in perceptual quality and realistic texture reconstruction. (3) Previous RefSR methods exhibit inferior performance on images with realistic degradations compared to GAN-based SISR models. This is largely due to the reliance on patch-matching correspondence networks, which become unreliable under complex or unknown degradations. In contrast, our RefDSR model leverages a diffusion-based architecture to enable more robust and reliable reference utilization, making RefSR truly effective in the presence of realistic degradations.

In the given-reference setting, the model directly uses a high-quality reference image without requiring a retriever. We evaluate our RefSR generator RefDSR on the WR-SR test set and compare it with other diffusion-based methods. As shown in Tab. 2, RefDSR consistently outperforms all other methods in both fidelity and perceptual quality, demonstrating the effectiveness of our approach.

Qualitative Comparison. Fig. 4 presents visual compar-

Method	PSNR \uparrow	SSIM \uparrow	LPIPS \downarrow	FID \downarrow	NIQE \downarrow
DiffBIR	21.75	0.5426	0.3854	79.36	4.3015
SeeSR	21.76	0.5677	0.3530	65.01	3.8409
OSEDiff	21.88	0.5746	0.3386	67.10	3.8338
Ours	21.92	0.5761	0.3254	57.82	3.6509

Table 2: Quantitative comparison with diffusion-based methods on WR-SR test set.

isons of different diffusion-based SR methods. As illustrated in the first example, the input image contains an otter. StableSR fails to fully remove noise, DiffBIR does not reconstruct the correct otter structure, and PASD produces overly smooth textures lacking fine details. Although SeeSR and OSEDiff leverage degradation-aware semantic cues to generate reasonable results, they still lack realistic details, making their outputs appear less natural. In contrast, RASR-Net successfully reconstructs richer fur textures while also generating a more realistic nose and mouth, resulting in a faithful and visually compelling restoration. A similar trend is observed in the second example. StableSR incorrectly interprets the noisy background as a mountain, DiffBIR fails to generate the correct structure of the peacock, and PASD again produces overly smoothed textures. SeeSR and OSEDiff deliver reasonable but detail-lacking results. RASR-Net, however, reconstructs finer head textures and neck feathers, achieving a more realistic and structurally accurate output. More visuals are provided in the supplementary.

Ablation Study

Effect of Text Prompt Conditioning. We conduct an ablation study to assess the impact of different text prompts on reconstruction quality, as shown in Tab. 3. During inference, using prompts from the LR image with a fine-tuned text extractor improves performance, but still fails in some cases (Wu et al. 2024b). Our results demonstrate that combining the LR-derived prompt with the retrieved reference prompt enhances visual fidelity and texture realism, outperforming either prompt alone. This validates our approach of combining input and reference information for more robust conditioning in generation.

Prompt	PSNR \uparrow	LPIPS \downarrow	FID \downarrow	CLIQQA \uparrow
\emptyset	23.65	0.3461	75.60	0.7436
LR	23.64	0.3315	61.37	0.7620
REF	23.67	0.3276	57.79	0.7627
REF+LR	23.67	0.3273	56.83	0.7706

Table 3: Ablation study on text prompt conditioning.

Effectiveness of Loss Components. We conduct an ablation study to assess the impact of Gram and GAN losses, as shown in Tab. 4. Training with only MSE and LPIPS provides limited texture supervision, resulting in suboptimal perceptual quality. Incorporating the Gram loss improves

perceptual metrics related to texture consistency and style. The GAN loss further enhances perceptual realism, yielding significant gains in no-reference quality measures and overall visual naturalness. Combining both losses achieves the best perceptual performance, demonstrating the benefit of combining style and adversarial supervision.

λ_{Gram}	λ_{GAN}	PSNR \uparrow	FID \downarrow	NIQE \downarrow	CLIQQA \uparrow
\emptyset	\emptyset	24.35	59.99	4.4543	0.7133
\checkmark	\emptyset	23.96	60.47	4.2639	0.7565
\emptyset	\checkmark	23.70	56.79	4.1848	0.7588
\checkmark	\checkmark	23.67	56.83	4.1139	0.7706

Table 4: Different results using different losses.

Retrieval Encoder Comparison. Tab. 5 reports a quantitative comparison of different retrieval encoders. The baseline without any retrieval encoder (denoted as None) randomly selects a reference image, resulting in poor fidelity and perceptual quality. VGG16-based (Simonyan and Zisserman 2014) retrieval outperforms random selection. However, its reliance on low-level texture features makes it sensitive to degradations in LR images, leading to lower fidelity and perceptual performance compared to semantic-based encoders such as CLIP (Radford et al. 2021) and DINOv2 (Oquab et al. 2023). Among them, DINOv2 achieves the best LPIPS, FID, and CLIQQA scores. Therefore, we adopt DINOv2 as the default retrieval encoder.

Encoder	PSNR \uparrow	LPIPS \downarrow	FID \downarrow	CLIQQA \uparrow
None	23.47	0.3594	81.25	0.7613
VGG16	23.61	0.3338	59.70	0.7676
CLIP	23.68	0.3283	56.73	0.7660
DINOv2	23.67	0.3273	56.83	0.7706

Table 5: Different results using different retrieval encoders.

Complexity Analysis

Our RefDSR model has 12.8M trainable parameters and an inference time of 0.15 seconds, compared to 0.10 seconds for the SISR baseline. To evaluate retrieval overhead, we use the LSDIR dataset (84,991 HR images) to build a Qdrant-based ² vector database. The average retrieval time for a given LR input is 0.15 seconds. All experiments are conducted on an A800 GPU with 512×512 input images.

Conclusion

In this paper, we propose RASR, a retrieval-augmented paradigm for practical reference-based image restoration. It integrates semantic retrieval from a reference database to eliminate the need for curated target-reference image pairs required by current RefSR methods. To advance research in this domain, we construct RASR-Flickr30, the first

²<https://qdrant.tech/>

benchmark with per-category reference databases for open-world retrieval. Our proposed baseline, RASRNet, combines semantic retrieval with a diffusion-based generator and demonstrates clear improvements over SISR baselines. These results underscore the potential of retrieval augmentation in bridging the gap between academic RefSR research and real-world applications. Despite promising results, there remains potential for improved reference fusion. Moreover, RASRNet exhibits limitations in restoring fine details such as scene text and subtle semantics. These issues will be addressed in future work.

References

- Barnes, C.; Shechtman, E.; Finkelstein, A.; and Goldman, D. B. 2009. PatchMatch: A randomized correspondence algorithm for structural image editing. *ACM Trans. Graph.*, 28(3): 24.
- Cao, J.; Liang, J.; Zhang, K.; Li, Y.; Zhang, Y.; Wang, W.; and Gool, L. V. 2022. Reference-based image super-resolution with deformable attention transformer. In *European conference on computer vision*, 325–342. Springer.
- Caron, M.; Touvron, H.; Misra, I.; Jégou, H.; Mairal, J.; Bojanowski, P.; and Joulin, A. 2021. Emerging properties in self-supervised vision transformers. In *Proceedings of the IEEE/CVF international conference on computer vision*, 9650–9660.
- Chen, X.; Wang, X.; Zhou, J.; Qiao, Y.; and Dong, C. 2023. Activating more pixels in image super-resolution transformer. In *Proceedings of the IEEE/CVF conference on computer vision and pattern recognition*, 22367–22377.
- Dai, J.; Qi, H.; Xiong, Y.; Li, Y.; Zhang, G.; Hu, H.; and Wei, Y. 2017. Deformable convolutional networks. In *Proceedings of the IEEE international conference on computer vision*, 764–773.
- Ding, K.; Ma, K.; Wang, S.; and Simoncelli, E. P. 2020. Image quality assessment: Unifying structure and texture similarity. *IEEE transactions on pattern analysis and machine intelligence*, 44(5): 2567–2581.
- Heusel, M.; Ramsauer, H.; Unterthiner, T.; Nessler, B.; and Hochreiter, S. 2017. Gans trained by a two time-scale update rule converge to a local nash equilibrium. *Advances in neural information processing systems*, 30.
- Hu, E. J.; Shen, Y.; Wallis, P.; Allen-Zhu, Z.; Li, Y.; Wang, S.; Wang, L.; Chen, W.; et al. 2022. Lora: Low-rank adaptation of large language models. *ICLR*, 1(2): 3.
- Huang, J.-B.; Singh, A.; and Ahuja, N. 2015. Single image super-resolution from transformed self-exemplars. In *Proceedings of the IEEE conference on computer vision and pattern recognition*, 5197–5206.
- Jiang, Y.; Chan, K. C.; Wang, X.; Loy, C. C.; and Liu, Z. 2021. Robust reference-based super-resolution via c2-matching. In *Proceedings of the IEEE/CVF Conference on Computer Vision and Pattern Recognition*, 2103–2112.
- Ke, J.; Wang, Q.; Wang, Y.; Milanfar, P.; and Yang, F. 2021. Musiq: Multi-scale image quality transformer. In *Proceedings of the IEEE/CVF international conference on computer vision*, 5148–5157.
- Kumari, N.; Zhang, R.; Shechtman, E.; and Zhu, J.-Y. 2022. Ensembling off-the-shelf models for gan training. In *Proceedings of the IEEE/CVF conference on computer vision and pattern recognition*, 10651–10662.
- Li, Y.; Zhang, K.; Liang, J.; Cao, J.; Liu, C.; Gong, R.; Zhang, Y.; Tang, H.; Liu, Y.; Demandolx, D.; et al. 2023. Lsdir: A large scale dataset for image restoration. In *Proceedings of the IEEE/CVF Conference on Computer Vision and Pattern Recognition*, 1775–1787.
- Liang, J.; Cao, J.; Sun, G.; Zhang, K.; Van Gool, L.; and Timofte, R. 2021. Swinir: Image restoration using swin transformer. In *Proceedings of the IEEE/CVF international conference on computer vision*, 1833–1844.
- Lin, X.; He, J.; Chen, Z.; Lyu, Z.; Dai, B.; Yu, F.; Qiao, Y.; Ouyang, W.; and Dong, C. 2024. Diffbir: Toward blind image restoration with generative diffusion prior. In *European Conference on Computer Vision*, 430–448. Springer.
- Liu, Z.; Lin, Y.; Cao, Y.; Hu, H.; Wei, Y.; Zhang, Z.; Lin, S.; and Guo, B. 2021. Swin transformer: Hierarchical vision transformer using shifted windows. In *Proceedings of the IEEE/CVF international conference on computer vision*, 10012–10022.
- Loshchilov, I.; and Hutter, F. 2017. Decoupled weight decay regularization. *arXiv preprint arXiv:1711.05101*.
- Matsui, Y.; Ito, K.; Aramaki, Y.; Fujimoto, A.; Ogawa, T.; Yamasaki, T.; and Aizawa, K. 2017. Sketch-based manga retrieval using manga109 dataset. *Multimedia tools and applications*, 76: 21811–21838.
- Oquab, M.; Darcet, T.; Moutakanni, T.; Vo, H.; Szafraniec, M.; Khalidov, V.; Fernandez, P.; Haziza, D.; Massa, F.; El-Nouby, A.; et al. 2023. Dinov2: Learning robust visual features without supervision. *arXiv preprint arXiv:2304.07193*.
- Radford, A.; Kim, J. W.; Hallacy, C.; Ramesh, A.; Goh, G.; Agarwal, S.; Sastry, G.; Askell, A.; Mishkin, P.; Clark, J.; et al. 2021. Learning transferable visual models from natural language supervision. In *International conference on machine learning*, 8748–8763. PmLR.
- Shim, G.; Park, J.; and Kweon, I. S. 2020. Robust reference-based super-resolution with similarity-aware deformable convolution. In *Proceedings of the IEEE/CVF conference on computer vision and pattern recognition*, 8425–8434.
- Simonyan, K.; and Zisserman, A. 2014. Very deep convolutional networks for large-scale image recognition. *arXiv preprint arXiv:1409.1556*.
- Sun, L.; and Hays, J. 2012. Super-resolution from internet-scale scene matching. In *2012 IEEE International conference on computational photography (ICCP)*, 1–12. IEEE.
- Wang, J.; Chan, K. C.; and Loy, C. C. 2023. Exploring clip for assessing the look and feel of images. In *Proceedings of the AAAI conference on artificial intelligence*, volume 37, 2555–2563.
- Wang, J.; Yue, Z.; Zhou, S.; Chan, K. C.; and Loy, C. C. 2024a. Exploiting diffusion prior for real-world image super-resolution. *International Journal of Computer Vision*, 132(12): 5929–5949.

- Wang, X.; Xie, L.; Dong, C.; and Shan, Y. 2021. Real-esrgan: Training real-world blind super-resolution with pure synthetic data. In *Proceedings of the IEEE/CVF international conference on computer vision*, 1905–1914.
- Wang, Y.; Yang, W.; Chen, X.; Wang, Y.; Guo, L.; Chau, L.-P.; Liu, Z.; Qiao, Y.; Kot, A. C.; and Wen, B. 2024b. Sinsr: diffusion-based image super-resolution in a single step. In *Proceedings of the IEEE/CVF conference on computer vision and pattern recognition*, 25796–25805.
- Wu, R.; Sun, L.; Ma, Z.; and Zhang, L. 2024a. One-step effective diffusion network for real-world image super-resolution. *Advances in Neural Information Processing Systems*, 37: 92529–92553.
- Wu, R.; Yang, T.; Sun, L.; Zhang, Z.; Li, S.; and Zhang, L. 2024b. Seesr: Towards semantics-aware real-world image super-resolution. In *Proceedings of the IEEE/CVF conference on computer vision and pattern recognition*, 25456–25467.
- Yang, F.; Yang, H.; Fu, J.; Lu, H.; and Guo, B. 2020. Learning texture transformer network for image super-resolution. In *Proceedings of the IEEE/CVF conference on computer vision and pattern recognition*, 5791–5800.
- Yang, T.; Wu, R.; Ren, P.; Xie, X.; and Zhang, L. 2024. Pixel-aware stable diffusion for realistic image super-resolution and personalized stylization. In *European Conference on Computer Vision*, 74–91. Springer.
- Yu, F.; Gu, J.; Li, Z.; Hu, J.; Kong, X.; Wang, X.; He, J.; Qiao, Y.; and Dong, C. 2024. Scaling up to excellence: Practicing model scaling for photo-realistic image restoration in the wild. In *Proceedings of the IEEE/CVF conference on computer vision and pattern recognition*, 25669–25680.
- Zhang, K.; Liang, J.; Van Gool, L.; and Timofte, R. 2021. Designing a practical degradation model for deep blind image super-resolution. In *Proceedings of the IEEE/CVF international conference on computer vision*, 4791–4800.
- Zhang, L.; Li, X.; He, D.; Li, F.; Ding, E.; and Zhang, Z. 2023. LMR: a large-scale multi-reference dataset for reference-based super-resolution. In *Proceedings of the IEEE/CVF International Conference on Computer Vision*, 13118–13127.
- Zhang, L.; Rao, A.; and Agrawala, M. 2023. Adding conditional control to text-to-image diffusion models. In *Proceedings of the IEEE/CVF international conference on computer vision*, 3836–3847.
- Zhang, L.; Zhang, L.; and Bovik, A. C. 2015. A feature-enriched completely blind image quality evaluator. *IEEE Transactions on Image Processing*, 24(8): 2579–2591.
- Zhang, R.; Isola, P.; Efros, A. A.; Shechtman, E.; and Wang, O. 2018. The unreasonable effectiveness of deep features as a perceptual metric. In *Proceedings of the IEEE conference on computer vision and pattern recognition*, 586–595.
- Zhang, Z.; Wang, Z.; Lin, Z.; and Qi, H. 2019a. Image super-resolution by neural texture transfer. In *Proceedings of the IEEE/CVF conference on computer vision and pattern recognition*, 7982–7991.
- Zhang, Z.; Wang, Z.; Lin, Z.; and Qi, H. 2019b. Image super-resolution by neural texture transfer. In *Proceedings of the IEEE/CVF conference on computer vision and pattern recognition*, 7982–7991.
- Zheng, H.; Ji, M.; Wang, H.; Liu, Y.; and Fang, L. 2018. Crossnet: An end-to-end reference-based super resolution network using cross-scale warping. In *Proceedings of the European conference on computer vision (ECCV)*, 88–104.